V
Displacements inside Oil Wells

V.1 Introduction

In the oil industry, operations such as: drilling, cementing, and completion of oil wells require a lot of material displacements. Particularly, in all of these operations, different materials are sequentially pumped into the well and the final quality of the operation is highly affected by the displacement efficiency. This is even more critical in wells where synthetic based material or oil based material is present, due to chemical incompatibility between the cement slurry and the drilling mud. For this reason, before executing an operation in a well, a detailed design including the optimization of the flow parameters and of the rheological properties of each material is essential to achieve success and guarantee the operational safety.

The success of these operations depends on the contamination between materials, on the position of the material inside the well, and on the dynamic pressures so as to secure that the operational window limits are respected. One of the main challenges in the design of an operation is to minimize the contamination between materials, and one way to evaluate the contamination is by the analysis of the shape of the interface between materials. A flat interface promotes an efficient displacement while elongate profiles usually result in material channelling. This analysis of the interface shape can be made by numerical simulations or experimental investigations.

The numerical simulation of flows is a powerful tool in the evaluation of different industrial process. Specifically in an oil well, where an experimental investigation is an expensive task, and sometimes not operationally feasible. Therefore, smaller scale experimental studies are usually conducted so as to validate the numerical results.

Most of the previous studies about the subject aimed at the representation of cementing operations, where complete fulfillment of the annular space with the cement slurry is a must for zonal isolation. Some works (Haut and Crook [88], [89]; Sauer [90]; Lockyear and Hibbert [91]) show that the process of material displacement through vertical oil wells is mainly governed by the viscosity ratio between materials, the eccentricity of the annular space between the column and the casing, the flow rate, and the density ratio.

Jakobsen et al. [92] analyzed experimentally the effects of viscosity ratio, buoyancy force and turbulence intensity in mud displacement through an eccentric annular tube. The results obtained show that the displacement is more efficient at the largest region, and that turbulence reduces the mud channeling at the narrowest region of the flow. Tehrani et al. [93] performed a theoretical and experimental study of laminar flow of drilling muds through eccentric annular spaces. They observed that, as the eccentricity increases, the displacement becomes worse. For vertical displacements, it was also shown that the process is more efficient for higher density differences between the displacer (higher density) and displaced material. Vefring et al. [94] analyzed, numerically and experimentally, the influence of rheological and flow parameters in the displacement of a drilling mud followed by cement slurry. The results obtained indicate that numerical simulations provide good results in this kind of problems.

Frigaard et al. [95], [96] presented some theoretical results of cement displacement through eccentric annuli, considering a two dimensional situation. They showed that the displacement front may reach permanent regime for some combinations of physical properties. For these cases, an analytical expression for the interface shape was obtained.

Guillot et al. [97] performed a theoretical approximate analysis of the flow of a washer material pushing a drilling mud through eccentric annuli. All the results were obtained with the washing material density greater than the mud density, and they concluded that turbulent flows present smoother interface shapes than the laminar ones.

Dutra et al. [98] analyzed numerically the flow of two adjacent materials through annular eccentric tubes. The effects of rheological parameters and eccentricity were investigated, for different flow rates. The results obtained show that the displacement is better when a more viscous material is used to push the other material. Also, it was observed that the interface shape is a function of flow regime and viscosities ratio. However, it is insensitive to eccentricity.

Since most of materials involved in these operations behave as a viscoplastic one, this chapter deals with material displacements inside oil wells. A numerical and experimental investigation was realized so as to determine in which conditions an effective displacement is obtained in order to clear up the phenomenon of material displacements inside oil wells.

V.2 Analysis

(a) Viscosity function and rheological parameters

Two kinds of materials were used in the experiments realized and in the numerical solution of the governing equations, Newtonian liquids and viscoplastic materials. Since it was considered that the temperature was constant in all experiments and numerical simulations, the viscosity of Newtonian liquids is constant (μ), as follows:

$$\eta = \mu \tag{1}$$

In order to describe the behavior of viscoplastic materials, two viscosity functions were used in the mathematical modelling: the SMD viscosity function proposed by de Souza Mendes and Dutra [24], and a regularized Herschel-Bulkley equation [48]. The SMD viscosity function is:

$$\eta = \left(1 - \exp\left[-\frac{\eta_o \dot{\gamma}}{\tau_o}\right]\right)\left(\frac{\tau_o}{\dot{\gamma}} + K\dot{\gamma}^{n-1}\right) \tag{2}$$

in this equation, $\dot{\gamma}$ is the shear rate, and the parameters η_o, τ_o, K, and n, are respectively the low shear rate viscosity, the yield stress, the consistency index, and the behavior or power-law index [24].

Defining $\dot{\gamma}_0 = \tau_0/\eta_0$, and $\dot{\gamma}_1 = (\tau_0/K)^{1/n}$, and choosing τ_0 as characteristic stress, and $\dot{\gamma}_1$ as characteristic shear rate, then

$$\tau^* = \frac{\tau}{\tau_0}; \qquad \dot{\gamma}^* = \frac{\dot{\gamma}}{\dot{\gamma}_1} \tag{3}$$

With Eq. (3) the SMD viscosity function can be written in the dimensionless form [25]:

$$\eta^* = \frac{\tau^*}{\dot{\gamma}^*} = \left(1 - \exp\left[-(J+1)\dot{\gamma}^*\right]\right)\left(\frac{1}{\dot{\gamma}^*} + \dot{\gamma}^{*n-1}\right) \tag{4}$$

where τ^* is the dimensionless shear stress, $\dot{\gamma}^*$ is the dimensionless shear rate, n is the behavior or power-law index, and J is the jump number given by the following expression:

$$J \equiv \frac{\dot{\gamma}_1 - \dot{\gamma}_o}{\dot{\gamma}_o} \tag{5}$$

And the regularized Herschel-Bulkley equation common used by the FLUENT software [48] can be written in the following form:

$$\eta = \frac{\tau_0 + k\left[\dot{\gamma}^n - \left(\frac{\tau_0}{\mu_0}\right)^n\right]}{\dot{\gamma}} \tag{6}$$

in this equation, $\dot{\gamma}$ is the shear rate, and the parameters μ_o, τ_o, K, and n, are respectively the yielding viscosity, the yield stress, the consistency index, and the behavior or power-law index.

(b) Governing parameters

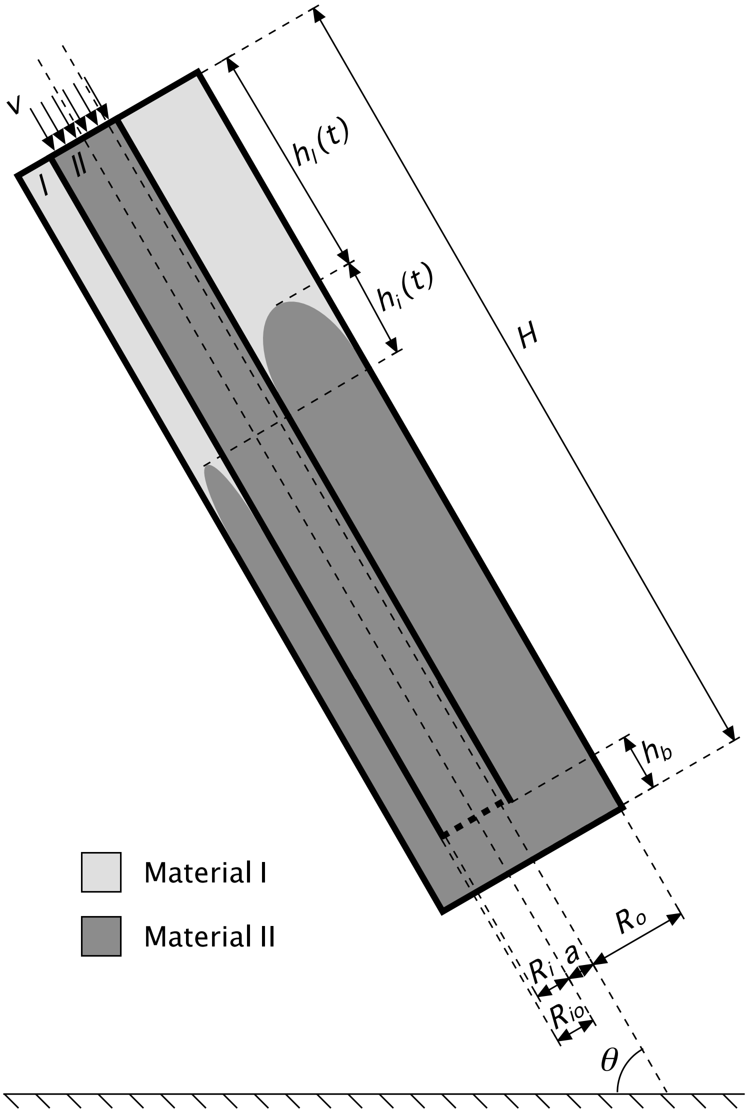

Figure V.1: The geometry.

The geometry considered is shown in Fig. V.1. The analysis of material displacements inside oil wells indicates that this flow is governed by seven dimensionless parameters. Two of these parameters depends only on the materials properties, the density ratio, ρ^*, and the viscosity ratio, η^*. There are also three geometrical parameters, namely, the radius ratio, R^*, the dimensionless eccentricity, e^*, and the dimensionless angle, θ^*. One other parameter that can affect the interface shape, and consequently the displacement efficiency is the dimensionless position of the interface, H^*, which is a function of time. The last parameter is a flow parameter, the dimensionless average velocity, $\bar{u}^*$. All of these parameters are defined as follows:

$$\rho^* = \frac{\rho_{II}}{\rho_I}; \qquad \eta^* = \frac{\eta_{II}}{\eta_I} \tag{7}$$

where ρ_{II} and η_{II} are respectively the density and the viscosity of the displacing material, and ρ_I and η_I are the density and the viscosity of the displaced one.

It is important to point out that if there is a viscoplastic material involved, the viscosity of this material can be defined as the viscosity evaluated at $\dot{\gamma} = \dot{\gamma}_1$.

The geometric parameters,

$$R^* = \frac{R_o}{R_i}; \quad e^* = \frac{(R_o - R_{io}) - a}{R_o - R_{io}}; \quad \theta^* = 1 - \frac{2\theta}{\pi} \tag{8}$$

where R_o and R_i are respectively the inner radius of the outer tube and the inner radius of the inner tube, R_{io} is the outer radius of the inner tube, a is the distance between the axis of the tubes, and θ is the angle defined at Fig. V.1.

And finally the dimensionless position of the interface, H^*, and the dimensionless average velocity, $\bar{u}^*$,

$$H^* = \frac{h_l}{H}; \qquad \bar{u}^* = \frac{\bar{u}}{(R_o - R_{io})\dot{\gamma}_1} \tag{9}$$

where $\bar{u}$ is the average velocity, R_o and R_{io} were previous defined, $\dot{\gamma}_1$ is the characteristic shear rate, H is the length of the outer tube and h_l is the position of the interface at the large size of the annulus.

V.3 Experimental Investigation

(a) Small scale experiments

The small scale apparatus consists of two glass tubes, one inside the other, forming the annular space, a polycarbonate box kept full with glycerol to eliminate image distortion, four pressurized reservoirs, two valve manifolds, and two laser equipments to provide the laser sheet. The experimental setup is illustrated in Fig. V.2. The apparatus dimensions and flow rates were chosen such that their dimensionless parameters match a typical real cementing operation [25]. The length of outer tube is 90 cm, while the inner-tube outside diameter is 16 mm, and the annulus gap is 9 mm.

Figure V.2: Small scale apparatus.

The experiment starts by filling the inner tube with the displacing material (Material 2), pressurizing its reservoir with the aid of compressed air and the valve manifolds VM1 and VM2. The annular space is then filled with the displaced material (Material 1) in a similar way. After this loading procedure, the connection gate between them is opened, allowing contact between the two materials and forming a flat interface. The displacement flow is then ready to start. The displacement process begins by pumping Material 2 through the inner tube so as to displace Material 1 in the annular space. Tracer particles (30μm in diameter) are mixed with Material 2. Two laser beams are employed to provide the visualization plane. The shape of the material-material interface front was photographed for different material rheologies and flow rates.

In these visualization experiments, the refraction index is an important parameter since reflections of the laser beam can appear in the pictures if the materials have different values from the refraction index of the tubes. This is one of the main problems in these experiments once a small difference in the refraction index of the materials employed can damage the pictures, making impossible to calculate the displacement efficiency by the interface shape. Therefore, in the first experiment glycerol was chosen as a Material 2 and a lower viscosity Newtonian oil with the same refraction index was chosen as the Material 1. In the second experiment a Carbopol dispersion was chosen as a Material 2, and a low viscosity oil as a Material 1. And in the third experiment, glycerol was chosen as a Material 2, and a Carbopol dispersion as a Material 1.

The main parameters that govern this flow are the orientation angle, the viscosity ratio, the density ratio, and the dimensionless flow rate. Due to the range of large gaps examined, the capillary force is not expected to play a significant role [82].

(b) Pilot scale experiments

The first pilot scale apparatus was built based on Dutra [99] and is illustrated in Fig. V.3. The experimental setup consists of one annular space constituted by two acrylic tubes, one inside the other, a visualization box filled up with glycerol, two pumps, and two reservoirs.

Table V.1: Properties of the materials used in apparatus 1.

Material	K (Pa.s^n)	n	τ_0 (Pa)
Drilling Mud	1.5705	0.4369	not available
Carbopol 0.08%	1.0443	0.48811	1.995
Spacer	4.788	0.25	not available
Carbopol 0.10%	4.9064	0.41741	12.444

The apparatus was built to allow the test section be inclined from 0^0 to 90^0. The outer-tube inside diameter was 92 mm, while the inner-tube inside diameter was 40 mm, and the annulus gap was 42 mm. The materials employed in the visualization displacement experiments were Carbopol aqueous dispersions with different concentrations in order to simulate the rheological behavior of a drilling mud and of a spacer material, as described in Tab. V.1. The experimental procedure was similar to the one adopted in the small scale experiments. First of all, the inner tube was filled with the displacing material (Material 2) with the aid of a pump. Then, the annular space was filled with the displaced material (Material 1) with the other pump. And finally, the connection gate was opened, and the displacing material was pumped. When the interface between the materials reached the visualization box, the pictures was taken with the aid of a CCD camera.

Figure V.3: Pilot scale apparatus 1.

Three cases were investigated in the pilot scale apparatus 1: (i) concentric annulus in the vertical position, (ii) concentric annulus inclined 45^0, and (iii) concentric annulus in the horizontal position. The results obtained will be presented in the next section.

Fig. V.4 shows a picture of the second pilot scale apparatus. Different from the pilot scale apparatus 1, in this apparatus there was no annular space region, just one acrylic tube was used. The tube was divided in two equal parts by a plate fixed inside the tube in one way to allow the visualization in both parts. The material entrance was located on the right side, where the downward displacement was analyzed, and the fluid exit was located on the left side, where the upward displacement occurred. The dimensions of the structure used were: 105 mm internal diameter and 1.5 m length. About 12.5 L of material were needed to fill up the tube illustrated in Fig. V.4.

Table V.2: Properties of the materials used in apparatus 2.

Material	Spacer	Cement Slurry	Water
Density (lb/gal)	8.2	16.4	8.34
Plastic Viscosity (cp)	40	234	1
Yield Stress (lbf/100 ft^2)	72	13	0
Correlation Coefficient (R)	0.9871	0.9994	1

The experiments realized in the apparatus 2 were two complete material replacement operations: (i) a cement slurry displacing a spacer material, and (ii) water displacing the cement slurry. The properties of the materials used are described in Table V.2. So, in this operations, the tube was initially filled up with the spacer material, then the cement slurry was pumped in order to replace the spacer material, and finally water was pumped to displace the cement slurry. The volume used to displace the material in the tube was 40 L, about 300% greater than the volume that would be required to replace all the material existing in the tube if the displacement were perfect.

Figure V.4: Pilot scale apparatus 2.

In these experiments, an evaluation of the displacement efficiency was made by measuring the density of the material samples collected in the exit of the tube. The measured values were compared with the theoretical ones that would be obtained if the displacement were perfect, i.e. if the displacing material could replace the displaced one without channeling and without mixture between them. The main objective of these second pilot scale experiments were to test a methodology of evaluating the displacement efficiency by measuring the density of the material collected in the exit of the tube in order to use the same methodology in the large scale experiments.

(c) Large scale experiments

As in the smaller scale apparatus, in the large scale physical simulations two concentric tubes were used. The external tube was $13\,\frac{3}{8}$ in casing, with internal diameter of $12\,\frac{1}{4}$ in. The inner-tube outside diameter was 5 in, while its inside diameter was $3\,\frac{3}{4}$ in. Fig. V.5 illustrates the structure that was built with an inclination angle of 45^0. The total length of the external casing tube was about 11 m, and the total volume of the structure, including the entry and exit lines, was about 6 bbl.

Figure V.5: Large scale apparatus.

In the large scale apparatus three physical simulations were performed, namely, (i) a material replacement physical simulation, (ii) a cement plug physical simulation 1, and (iii) a cement plug physical simulation 2.

Table V.3: Large scale physical simulation - material replacement.

Phase	Pumping Material	Volume (bbl)	ρ (lb/gal)	Yield Stress (lbf/100 ft^2)
0	Synthetic Based Drilling Mud	6	9.5	4
1	Spacer	8	11.4	30
2	Cement Slurry	8	16	52
3	Spacer	8	11.4	30

In the first physical simulation (i), three complete material replacement experiments were performed, as described in Table V.3. In the beginning of the experiments, the tube-annular region was filled up with the drilling mud with the aid of a pump. After that, a spacer material was pumped to the test section so as to replace the drilling mud. Then, the same procedure was adopted in order to replace the spacer material inside the tube-annular region by the cement slurry. And finally, the spacer material was pumped to replace the cement slurry. In the three replacement experiments decribed above, the flow rate used was 2 bbl/min, and the volume pumped of the displacing material was about 33% higher than the volume required to replace all the material inside the tube-annular region.

In the second physical simulation (ii), a balanced cement plug was designed in order to obtain 5 m of cement plug, 3 m of spacer above the cement, and 3 m of drilling mud above the spacer inside the outer tube, at the end of the simulation. The properties of the materials used in this physical simulation are presented in Table V.4, and the flow rate used in all the displacements described below was 2 bbl/min.

Table V.4: Large scale physical simulation - cement plug 1.

Material	Drilling Mud	Spacer	Cement Slurry
Density (lb/gal)	10	12.1	16.1
Plastic Viscosity (cp)	45	32	637
Yield Stress (lbf/100 ft^2)	7	26	48
Correlation Coefficient (R)	1.000	0.9966	0.9998

In this phisycal simulation (ii), the tube-annular region was filled up with the drilling mud, in the beginning of the experiment. Then, the designed volumes of the spacer material, and of the cement slurry were sequentially pumped into the test section, followed by pumping, in order, the remaining amount of the spacer material, and of the drilling mud. Finally, just after pumping all materials, the inner tube was carefully removed from the test section, and after the cement slurry has been cured the composition inside the outer tube of the physical simulation (ii) was analyzed.

In the third physical simulation (iii), a cement plug was designed with the same volumes as the ones used in the cement plug 1 physical simulation (ii). Therefore, the materials volume pumped was enough to obtain 5 m of cement, 3 m of spacer above the cement, and 3 m of drilling mud above the spacer inside the outer tube, at the end of the simulation (iii). The spacer used in this simulation (iii) was different from the one used in the previous test (ii). The properties of the materials used in the cement plug 2 physical simulation (iii) are presented in Table V.5. All the procedures in this simulation (iii) were the same as the ones adopted in the previous cement plug physical simulation (ii).

Table V.5: Large scale physical simulation - cement plug 2.

Material	Drilling Mud	Spacer	Cement Slurry
Density (lb/gal)	10.7	8.1	16.1
Plastic Viscosity (cp)	56	33	182
Yield Stress (lbf/100 ft^2)	17	86	70
Correlation Coefficient (R)	0.9999	0.9986	0.9994

(d) Rheological measurements

As explained before, the knowledge of the rheological properties of each material used in displacement experiments is fundamental to better understand the displacement efficiency in each situation. Therefore, in each apparatus, a number of displacement experiments were performed, and the materials used in each experiment were rheologically characterized in an specific way.

The measurements of the rheological properties of the materials used in the small scale apparatus were done with the aid of an AR-G2 rheometer. The viscosity of both Newtonian liquids was measured with a smooth concentric cylinder geometry, while the flow curve of the Carbopol dispersion was measured with a cross-hatched plates geometry so as to avoid apparent slip.

In the pilot scale apparatus 1 experiments, two aqueous Carbopol dispersions was used. The characterization of the rheological properties of each dispersion was realized using an ARES rheometer and a grooved Couette geometry in order to avoid apparent slip. At last, all the materials used in the pilot scale apparatus 2, and in the large scale apparatus had their rheological properties characterized with a Fann rheometer, according the API procedures.

V.4 Numerical Solution

Numerical solutions were obtained for comparison with the experiments realized in the pilot scale apparatus 1, and in the large scale physical simulation. In the numerical solutions of the cases corresponding to the pilot scale apparatus 1 experiments, the generalized material constitutive equation was used with the SMD viscosity function [24]. On the other hand, in the numerical solutions of the cases corresponding to the experiments realized in the large scale apparatus, a regularized Bingham equation was employed [48].

In the numerical solutions of the governing equations, the finite volume method described by Patankar [62] was used to discretize the conservation equations of mass and momentum. The SIMPLE algorithm [62] was used to calculate the coupled velocity and pressure fields, and the volume of fluid method (VOF) [100] was used to calculate the volume fraction of each phase in the entire domain, i.e. to calculate the volume fraction of the phases in each cell of the domain.

In all cases studied in this chapter, from the numerical solution of the governing equations and from the information of the volume of fraction of the phases in all cells, the interface shape between different materials was obtained for each time step. Depending on the case studied, a tri-dimensional or a bi-dimensional mesh was created and tested so as to simulate the transient flow and guarantee that the numerical solution was independent of the mesh (error $\leq 0.1\%$).

V.5 Results and Discussion

(a) Small scale

The cases presented here pertain to the vertical concentric annulus case. The flow is downwards in the tube and upwards in the annular space.

The first case studied (i) involves two Newtonian liquids with almost the same refraction index of the tubes so as to turn easier the development of the technique of taking good pictures, and improve their quality. The interface shape evolution for this case of one Newtonian liquid displacing another is illustrated in Fig. V.6. This figure shows pictures of the interface at different times. For this case, Material 2 is glycerol and Material 1 is a lower viscosity oil. No similar pictures, showing an interface shape evolution in an annular space, using a laser sheet to eliminate curvature effects, was found in the literature. The viscosity ratio $N_\mu = \mu_1/\mu_2$ was $\simeq 8$ and the density ratio was around 1.36. It can be seen that, for this combination of parameters, the interface evolves to a fixed shape, and the displacement efficiency is nearly 100%.

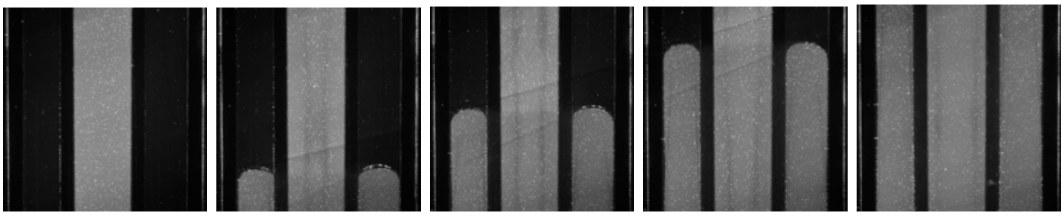

Figure V.6: Interface evolution. Newtonian liquid 2 (glycerol) displacing a Newtonian liquid 1 (lower viscosity oil). Time increases from left to right.

The cases involving viscoplastic materials employ Carbopol 0,13% dispersion in a water-glycerol mixture with 50% of glycerol in weight. Glycerol was added in the Carbopol dispersion so as to increase the refraction index of the viscoplastic material, trying to minimize the reflections of the laser beam and improve the quality of the pictures. The low viscosity oil, and the glycerol used in these cases were the same as the ones used in the first case (i). Two such cases are examined, namely: (ii) Material 2 is viscoplastic while Material 1 is Newtonian; and (iii) Material 2 is Newtonian while Material 1 is viscoplastic.

Fig. V.7 illustrate the interface evolution of the second case (ii), showing a Carbopol dispersion displacing a low viscosity Newtonian oil. The quality of these pictures, in Fig. V.7, was not so good as the ones obtained in the first case (Fig. V.6). This happened due to reflections of the laser beam caused by a small difference in the refraction index of the Carbopol dispersion compared to the refraction index of the tube. Nevertheless, it is possible to observe that for this combination of parameters the interface shape is flat, corresponding to an excellent displacement efficiency, nearly 100%.

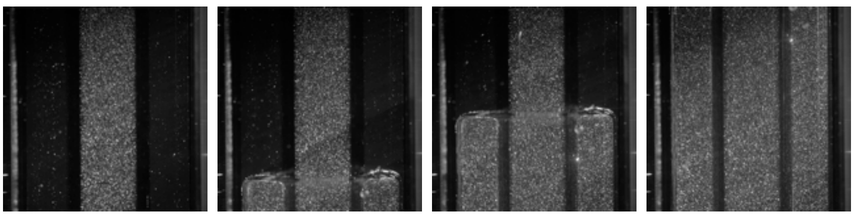

Figure V.7: Interface evolution. Viscoplastic material (Carbopol dispersion) displacing a Newtonian liquid (low viscosity oil). Time increases from left to right.

Fig. V.8 shows the interface evolution for the third case, a Newtonian liquid displacing a Carbopol dispersion. Despite not damaging the pictures, as in the second case, reflections of the laser beam appear in the images of the third case, due to the refraction index of the Carbopol dispersion. Different from the previous cases, (i) and (ii), in the third case (iii) the displacement efficiency was not good. In this case, of one Newtonian liquid displacing a viscoplastic material with a fixed flow rate, a preferable way through the Carbopol dispersion was found by the glycerol due to interface instability cause by the viscosity ratio. Thus, a big amount of Carbopol dispersion stay in the annular space, and the displacement efficiency was not good.

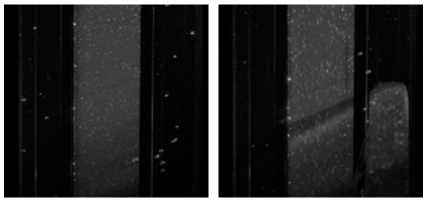

Figure V.8: Interface evolution. Newtonian liquid (glycerol) displacing a Viscoplastic material (Carbopol dispersion). Time increases from left to right.

(b) Pilot scale

Three cases were investigated in the pilot scale apparatus 1. In all of the experiments a Carbopol 0.10% dispersion displaced a Carbopol 0.08%. In the first case the annulus was concentric and in the vertical position. In the second case, the annulus was inclined 45^0, and in the third case the annulus was in the horizontal position. Numerical results were obtained by solving the governing equations as described in Sec. V.4 and will be compared with the experimental results.

Fig. V.9 shows pictures of the interface evolution for the vertical case studied in the pilot scale apparatus 1. By the analysis of these images, it is possible to observe that the interface shape between the Carbopol 0.10% (the blue material) and the Carbopol 0.08% (the white one) is flat, corresponding to an efficient displacement. It is also observed that in a few instants of time all the Carbopol 0.08% was replaced by the Carbopol 0.10% indicating that the displacement efficiency was nearly 100%.

The pictures pertained to the second case, with the apparatus in the inclined position, are presented in Fig. V.10. Analyzing the images, it is observed that the symmetry expected in the interface was not obtained. This asymmetry is due to the difficult in forming a flat interface perpendicular to the flow direction in the beginning of the experiment, and has nothing to do with some difference in the density between the materials. In fact, both materials, Carbopol 0.10% and Carbopol 0.08%, have the same density.

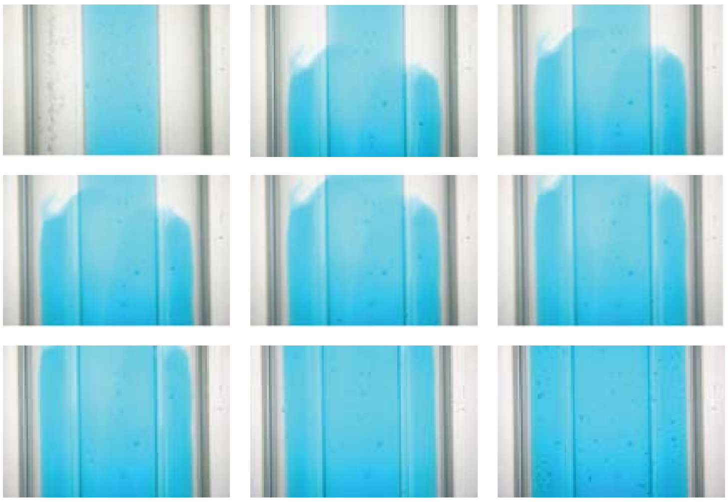

Figure V.9: Interface evolution for the vertical case (0^0). Carbopol 0.10% (blue) displacing Carbopol 0.08% (white). Time increases from left to right, and from the top to the bottom.

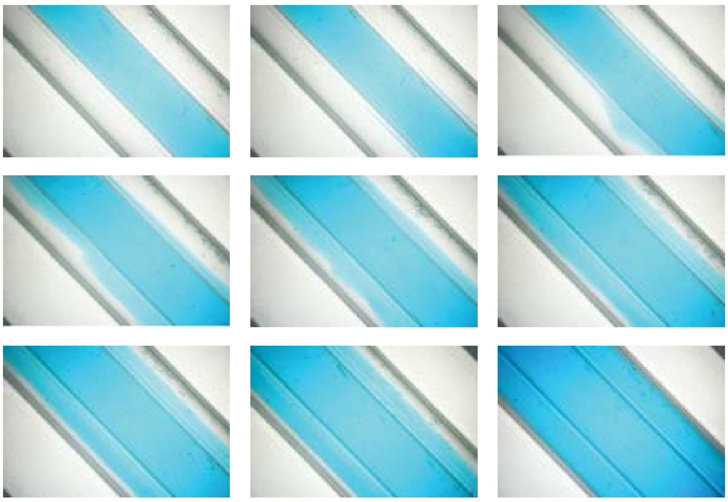

Figure V.10: Interface evolution for the inclined case (45^0). Carbopol 0.10% (blue) displacing Carbopol 0.08% (white). Time increases from left to right, and from the top to the bottom.

It is also observed that the interface shape, in the inclined case, is sharper than the interface in the vertical case. Although the interface is shaper in the inclined case, and the displacement occurred first in the bottom of the annulus due to the asymmetry, in the same pumping time all the Carbopol 0.10% replaced the Carbopol 0.08%, indicating a displacement efficiency nearly 100%.

Fig. V.11 shows the images of the horizontal case. As in the inclined case, the interface shape is sharper than the one obtained in the vertical case. Since both materials have the same density, and in the beginning of the experiment the interface was similar to the one obtained in the inclined case, it was expected that the displacement occurred first in the bottom. However, in an unexpected way the displacement occurred first in the top of the annulus, different from the inclined case. This happened due to an eccentricity in the middle of the annulus, caused by the weight of the inner tube, what turns easier the flow on the top of the annulus.

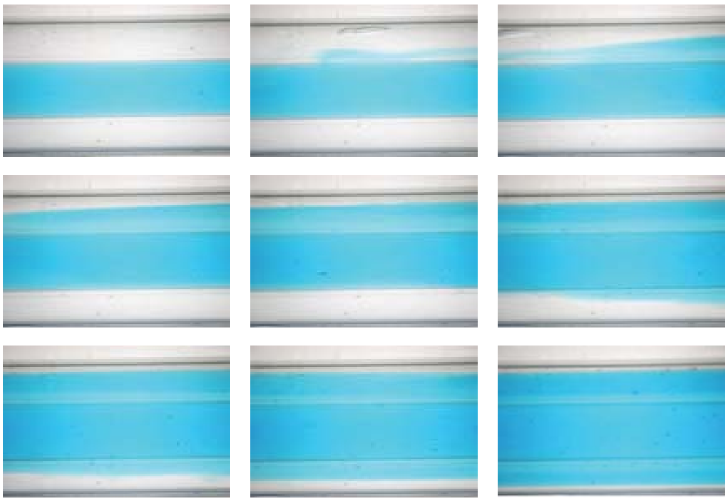

Figure V.11: Interface evolution for the horizontal case (90^0). Carbopol 0.10% (blue) displacing Carbopol 0.08% (white). Time increases from left to right, and from the top to the bottom.

Despite being asymmetric and sharper, it is possible to note in Fig. V.11 that the interface shape evolved to a good replacement in the same instant of time, indicating a displacement efficiency nearly 100%.

For comparison with the experimental results, some numerical simulation were performed by solving the governing equations according to Sec. V.4. Fig. V.12 shows both numerical – (a) and (b) – and experimental results – (c) and (d) – for the vertical case. In this figure and in the next ones, the Carbopol 0.08% is represented by the red color in the numerical results and by the blue color in the experimental results, while the Carbopol 0.10% is represented by the yellow and white colors respectively. By the analysis of the images it is possible to note that the interface shape is sharper in the numerical result – Fig. V.12 (a) – than the one obtained experimentally – Fig. V.12 (c). This observation can be explained by three hypothesis: (i) the interface shape in the experimental result was affected by curvature effects since there was no plan created in the middle of the annulus to take the picture, (ii) the Volume of Fluid method is not so good in predicting the interface shape, (iii) the experiment was affected by apparent wall slip.

Analyzing the hypothesis, the third one (iii) seems not to be occurred, once apparent wall slip manifests itself in the low shear rate range, and also it is possible to note, in the images, a thin layer of Carbopol 0.08% adjacent to the wall, indicating that the velocity is zero at the wall. In spite of not representing so well the interface shape, the numerical simulation predicted that in the same instant of the experimental time all the Carbopol 0.08% was replaced by the Carbopol 0,10%, as illustrated in Figs. V.12 (a) and (b). It represents a displacement efficiency nearly 100%.

(a) (c) (b) (d)

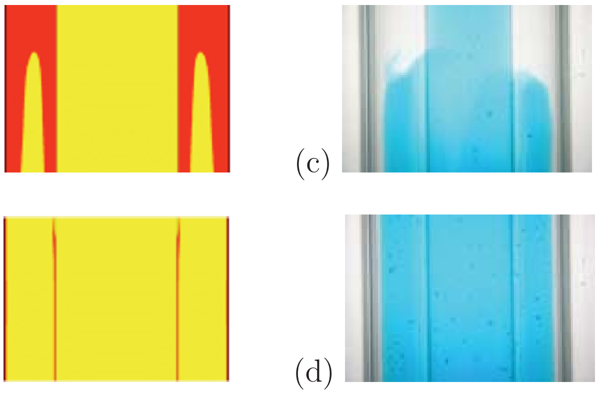

Figure V.12: Comparison between experimental and numerical results of Carbopol 0.10% displacing Carbopol 0.08% in the vertical case (0^0). (a) and (b) correspond to the numerical results. (c) and (d) correspond to the experimental results.

Fig. V.13 illustrate the images comparing the numerical results to the experimental results for the inclined case. It can be noted that the interface shape in this numerical result – Fig. V.13 (a) – is sharper than the one obtained in the vertical case – Fig. V.12 (a) as in the experimental result. The asymmetry obtained in the experimental result was due to the interface shape in the beginning, as explained above, and was not predicted by the numerical result. Also, in the numerical result it was predicted a thin layer of Carbopol 0.08% adjacent to the inner tube, which could not be evaluated by the experimental result due to curvature effects. At last, as in the vertical case, in the same instant of time, almost all the Carbopol 0.08% was replaced by the Carbopol 0.10%, indicating a displacement efficiency nearly 100%.

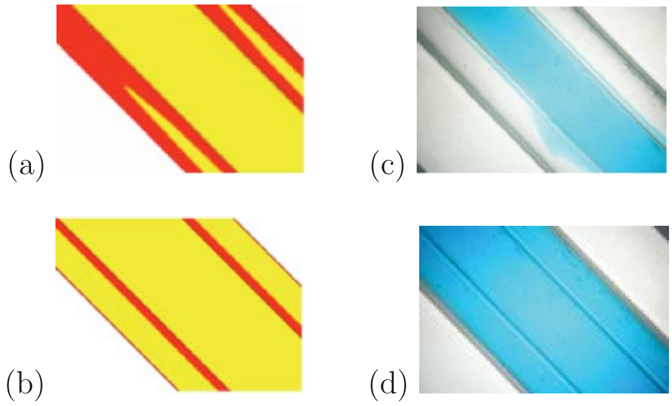

Figure V.13: Comparison between experimental and numerical results of Carbopol 0.10% displacing Carbopol 0.08% in the inclined case (45^0). (a) and (b) correspond to the numerical results. (c) and (d) correspond to the experimental results.

In Fig. V.14 it is shown the images comparing the numerical results to the experimental results for the horizontal case. Analyzing this images it is observed that the interface shape is sharper than the one obtained in the vertical case, as in the inclined case. The asymmetry in this case was due to the eccentricity created in the middle of the annulus, as explained before, and could not be predicted by the numerical simulation. Again, as in the inclined case, in the horizontal case a thin layer of Carbopol 0.08% was predicted by the numerical simulation and could not be verified by the experimental result due to curvature effects. And once more, in the same instant of experimental time, the numerical simulation predicted that almost all the Carbopol 0.08% would be replaced by the Carbopol 0.10%, what happened in the experimental result.

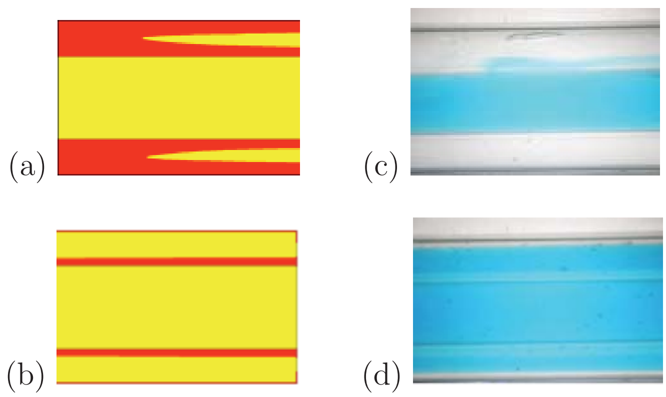

Figure V.14: Comparison between experimental and numerical results of Carbopol 0.10% displacing Carbopol 0.08% in the horizontal case (90^0). (a) and (b) correspond to the numerical results. (c) and (d) correspond to the experimental results.

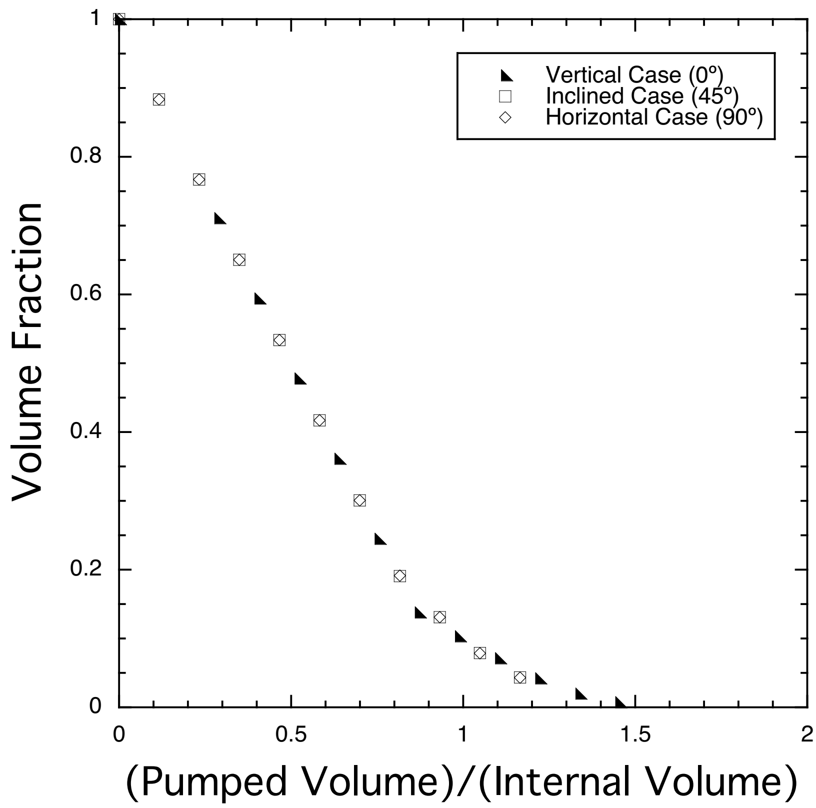

Figure V.15: Volume fraction of the Carbopol 0.08% for the three cases, calculated by the numerical solution.

Fig. V.15 shows the volume fraction of Carbopol 0.08% as a function of the ratio between the pumped volume by the internal volume, calculated by the numerical solution. By the analysis of this graphic it can be seen that if the displacement of the Carbopol 0.08% had been perfect, the volume fraction would have been equal to zero when the ration between the pumped volume by the internal volume was equal to one. So, the displacement was not perfect, but the displacement efficiency was nearly 90% when the ratio between the pumped volume by the internal volume was equal to one. By the same analysis, the displacement efficiency reached nearly 100% when the ratio between the pumped volume by the internal volume was equal to 1.5, condition which represents the experimental results. At last, it can be observed by Fig. V.15 that the displacement efficiency was not affected by the inclination angle, what was expected since both materials used had the same density.

The pilot scale 2 was used to perform two material displacement experiments, as described in Sec. V.3(b). In the first one, the tube was initially filled up with spacer material and then 40 L of the cement slurry was pumped to replace the spacer. And in the second experiment, water was pumped to displace the cement slurry inside the tube.

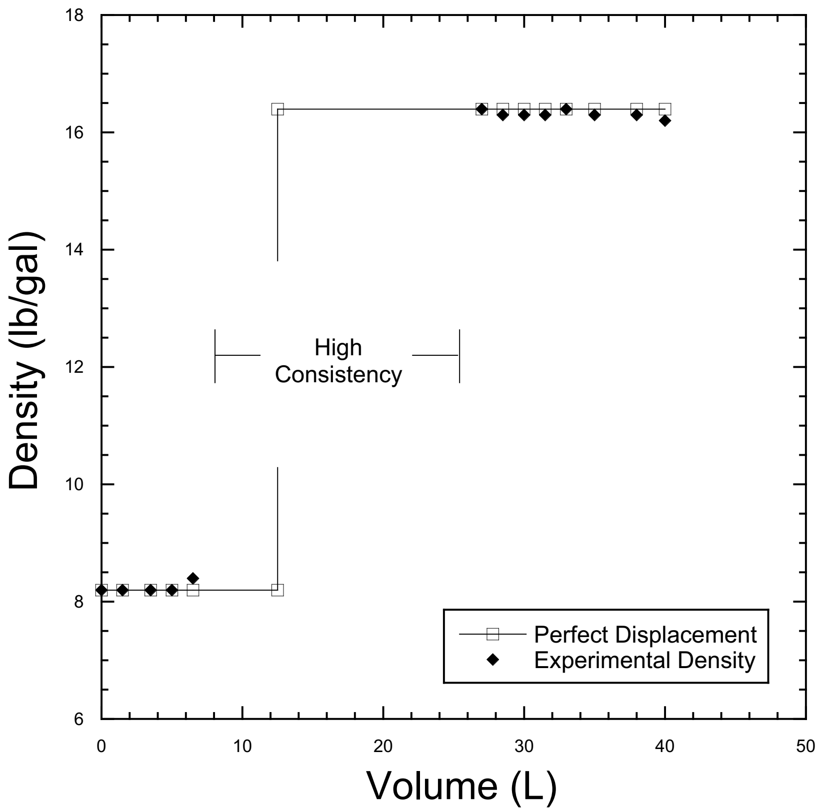

Figure V.16: Experimental density and the density that would be obtained if the displacement were perfect versus volume of cement slurry used to displace the spacer.

Fig. V.16 shows the measured density values of the samples collected in the exit of the tube related to the pumped volume of cement slurry, for the first experiment realized in the pilot scale apparatus 2. In this figure there is also illustrated the density values that would be obtained if the displacement were perfect, i.e. if no mixture between both materials occurred. Analyzing this figure it is possible to observe that in a perfect displacement of the spacer by the cement slurry, the density at the exit of the tube would keep the value of the spacer density (8.2 lb/gal) until 12.5 L of the cement slurry were pumped (the volume of the tube). After that, the density would change to the value of the cement slurry density (16.4 lb/gal). However, the viscosity of the mixture of materials at the exit increased abruptly after having pumped only 7 L of cement slurry, in such a way that it was no longer possible to perform either density or rheological parameter determination according to API procedures [101] in the high consistency range shown in Fig. V.16. The large increase in viscosity indicates the occurrence of a very incompatible mixture between the spacer and the cement slurry. Also, the displacement of the spacer by the cement slurry was not efficient, since it was necessary to pump approximately twice the ideal volume of the cement slurry (the volume of the tube) for the effluent density achieve the value of the cement slurry density (16.4 lb/gal).

(a)  (b)

Figure V.17: Displacement of the spacer (light color) by the cement slurry (black color). (a) Downward displacement, and (b) upward displacement.

(a)  (b)

Figure V.18: End of the displacement of the spacer (light color) by the cement slurry (black color). (a) Downward displacement, and (b) upward displacement.

Fig. V.17 shows pictures of the acrylic tube during the cement slurry pumping. This figure illustrate both the downward displacement, which represents what happens in the tube in a field operation, and the upward displacement, representing what occurs in the annulus of the well. In the downward displacement the cement slurry passes through the spacer (lighter color), due to the higher density and lower yield stress of the cement slurry compared to the spacer. The upward displacement shows an opposite behavior: no such channeling was produced through the spacer, i.e. the displacement was much more efficient due to the higher density of the cement slurry.

Fig. V.18 shows the situation at the end of the displacement. The downward displacement (a) was much more critical, the cement slurry created channels in the spacer which remained in the tube even after 40 L of cement slurry having been pumped. Results indicate that the upward displacement was much more effective, which is attributed to the higher density of the cement slurry.

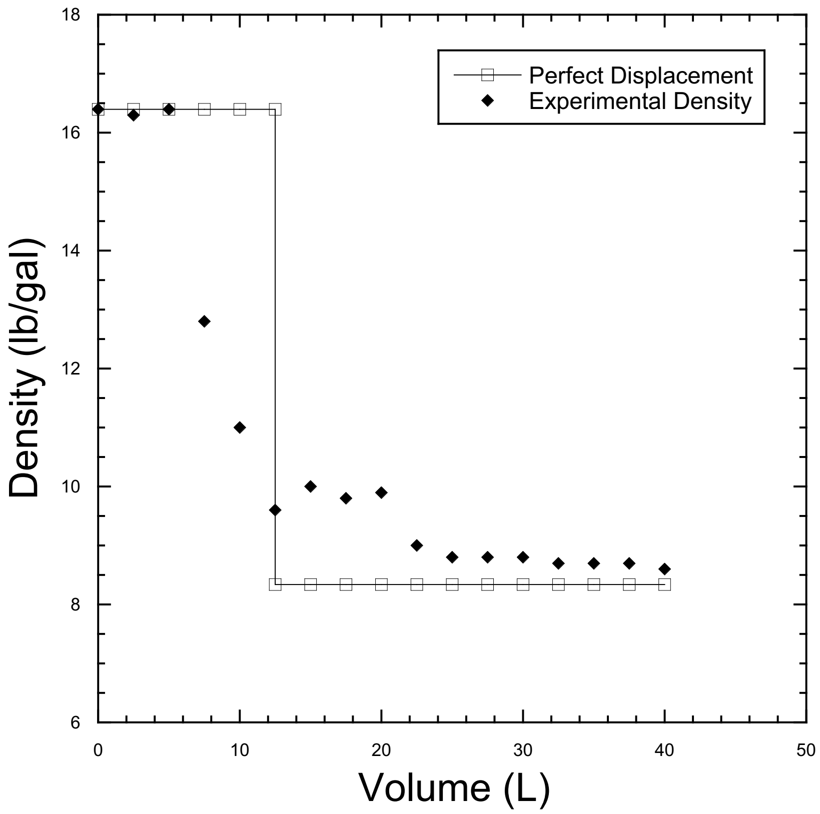

Figure V.19: Experimental density and the density that would be obtained if the displacement were perfect versus volume of water used to displace the cement slurry.

In the second experiment, executed in sequence of the first, 40 L of water were pumped into the tube to displace the cement slurry (and the spacer left in the tube). Fig. V.19 shows the variation of the density of the samples collected in the exit of the tube, and also the values of density that would be obtained if the displacement were perfect. In this figure, a reduction in the measured density is observed after 7.5 L of water was pumped. This behavior indicates that a channel was created through the cement slurry, since a reduction in the measured density was expected to occur when the pumped volume achieves 12.5 L.

(a) 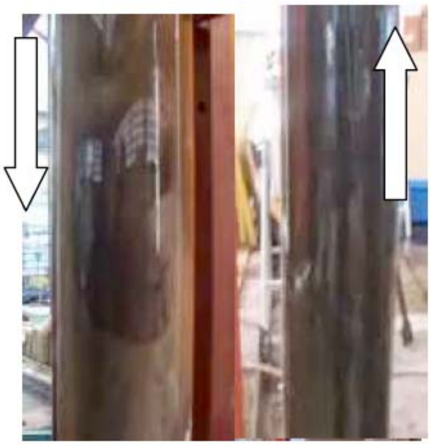 (b)

Figure V.20: Displacement of the cement slurry by water (13 L). (a) Downward displacement, and (b) upward displacement.

Finally, Fig. V.20 shows pictures of the acrylic tube during the pumping of water, more specifically after 13 L of water were pumped. In a perfect displacement the entire tube would be filled with water (which was not observed). There was cement left in both sides of the tube, indicating that the displacement was not efficient.

By a general analysis it is possible to observe that the displacement of one material by another having a much lower density (difference of about 8 lb/gal), and lower yield stress in laminar flow, resulted in severe channeling, indicating that the displacement was not efficient at all.

(c) Large scale

As described in Sec. V.3(c), the large scale apparatus was used to perform three physical simulations, namely, (i) a material replacement physical simulation, (ii) a cement plug physical simulation 1, and (iii) a cement plug physical simulation 2.

In the first physical simulation (i) three replacement experiments were sequentially realized, and the efficiency of the material replacement was evaluated based on the density of the material samples collected at the exit of the annulus. In the first one, the volume of 8 bbl of spacer were pumped to displace the drilling mud, previously pumped into the tube-annular region.

Fig. V.21 shows the experimental density, measured from the samples collected in different instants of time during the first replacement experiment, and the numerical density, calculated from the numerical solution with the FLUENT software. Fig. V.21 also show the density that would be obtained if the displacement were perfect for comparison with the experimental and numerical densities. By the analysis of this figure it is observed that in a perfect displacement a change in the density would be noted after pumping 6 bbl of the displacing material, since this was the internal volume of the structure. It is important to point out that in this first displacement experiment the density of the displaced material was 9.5 lb/gal while the density of the displacing one was 11.4 lb/gal.

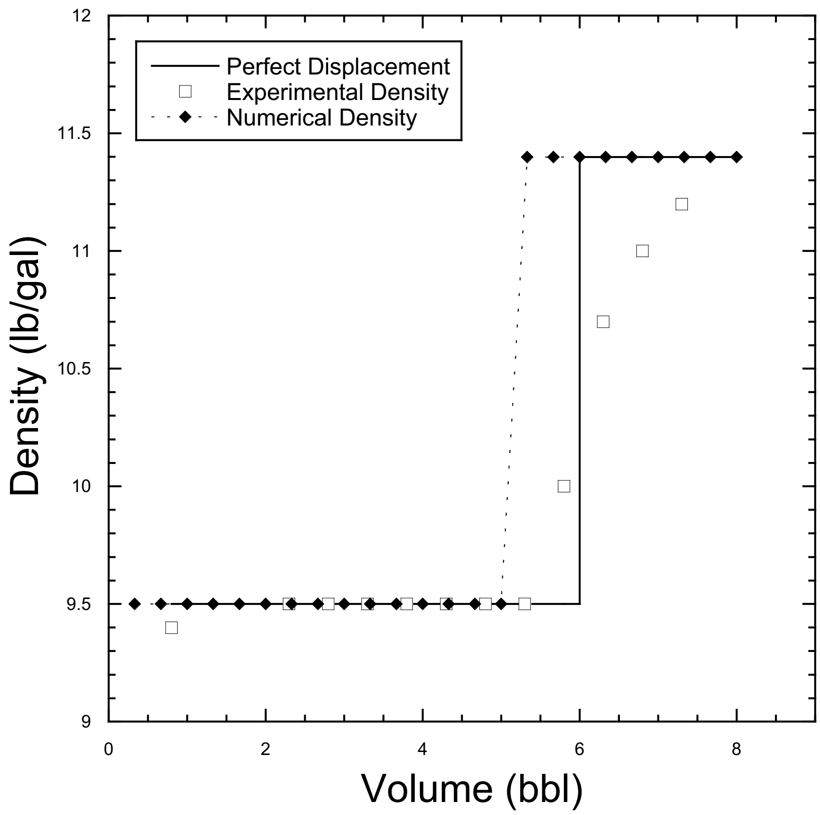

Figure V.21: Experimental and numerical densities versus volume of spacer used to displace the drilling mud, compared with the density that would be obtained if the displacement were perfect.

Looking into Fig. V.21 it can be seen an increase in the experimental density just before 6 bbl of spacer were pumped. In the same curve, just after

6 bbl of the spacer were pumped, the experimental density was slightly lower than expected by the perfect displacement, which means that no significant channeling of the spacer through the drilling mud occurred, indicating a good displacement efficiency. Comparing the experimental density with the numerical one it can be noted that the numerical results could predict an increase in the density before 6 bbl of spacer were pumped. However, the numerical density increased to 11.4 lb/gal before pumping 6 bbl of spacer which indicate that some little displaced material could not be removed. The experimental results also show that not all drilling mud was removed with the pumped volume equal to 8 bbl, but in this case the density increased slower than predicted by the numerical results. Although, both numerical and experimental results show a good displacement efficiency for this first replacement.

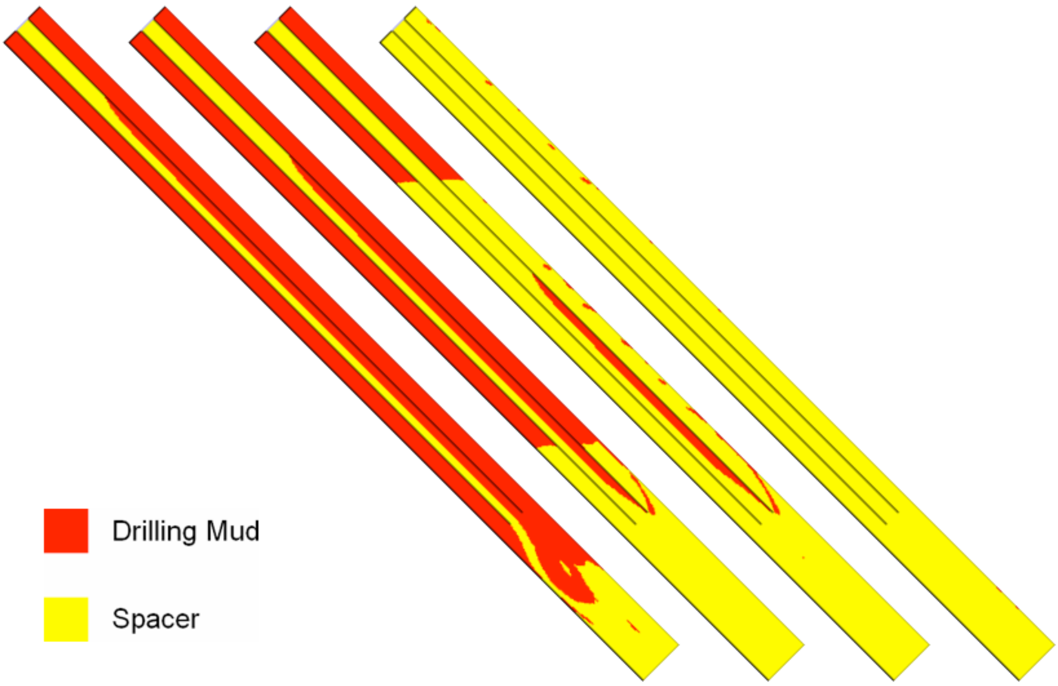

Figure V.22: Interface evolution of the displacement of the drilling mud by the spacer material predicted by the numerical solution of the governing equations.

Some images of the displacement obtained from the numerical solution of the governing equations for this first replacement are illustrated in Fig. V.22. In in this figure the displacement of the drilling mud by the spacer inside the tube-annular region is shown for four different instants of time: (i) when the spacer exits from the internal tube, (ii) in the beginning of the displacement in the annulus, (iii) in an advanced displacement in the annulus, and (iv) at the end of the pumping operation (after pumping 8 bbl of the spacer), when all the drilling mud should have been removed from the structure.

The numerical results of this first replacement agreed well with the experimental results since at the end of the displacement nearly all the drilling mud was removed both in the numerical and in the experimental results. Also, the interface shape in the numerical results was almost flat, indicating a good displacement efficiency which can be evaluated by the analysis of the experimental results in Fig. V.21. In this first replacement, the higher density and the higher yield stress of the spacer (11.4 lb/gal, and 30 lbf/100 ft^2) when compared to the drilling mud equivalent properties (9.6 lb/gal, and 4 lbf/100 ft^2) contributed to the good displacement efficiency.

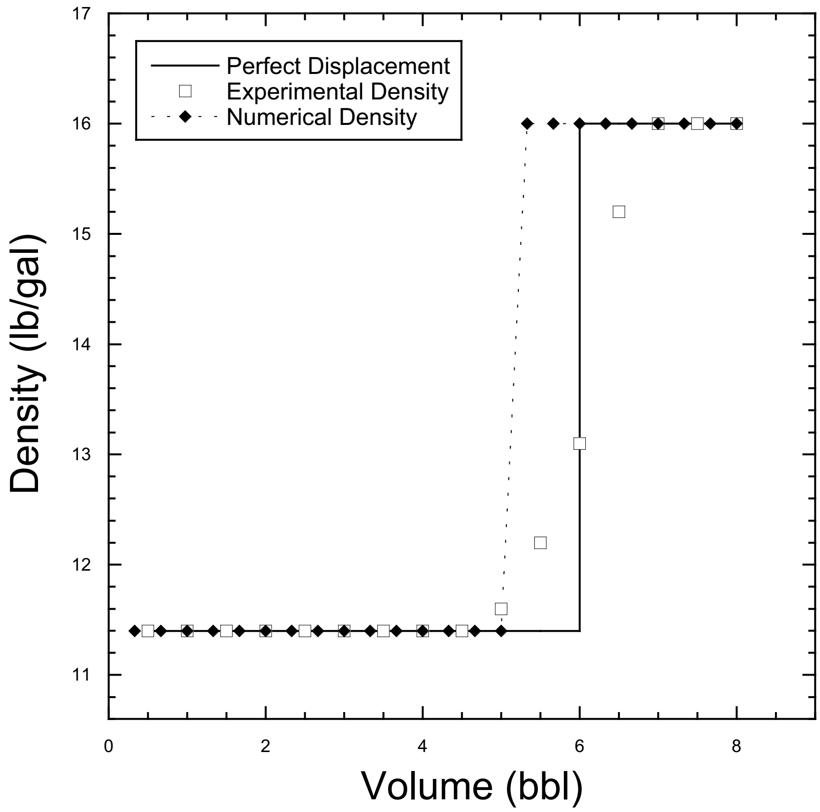

Figure V.23: Experimental and numerical densities versus volume of cement slurry used to displace the spacer, compared with the density that would be obtained if the displacement were perfect.

In the second experiment, realized just after the end of the first one, 8 bbl of cement slurry were pumped to displace the spacer. Fig. V.23 shows the experimental and numerical density values for this case, and a comparison with the density that would be obtained if the displacement were perfect. It is possible to observe in this figure that when 7 bbl of the cement slurry were pumped, the experimental density was equal to the cement slurry density, which means that all the spacer was replaced. Moreover, the experimental density was almost equal to the density that would be obtained if the displacement were perfect, indicating no channeling and an efficient displacement. As in the first displacement, the numerical results could predict an increase in the density before 6 bbl of cement slurry were pumped. The numerical solution also predicted that the displacer material density would be achieved before pumping 6 bbl of cement slurry, which did not happen in the experiment. Although, as in the first replacement, both numerical and experimental results indicate a good displacement efficiency.

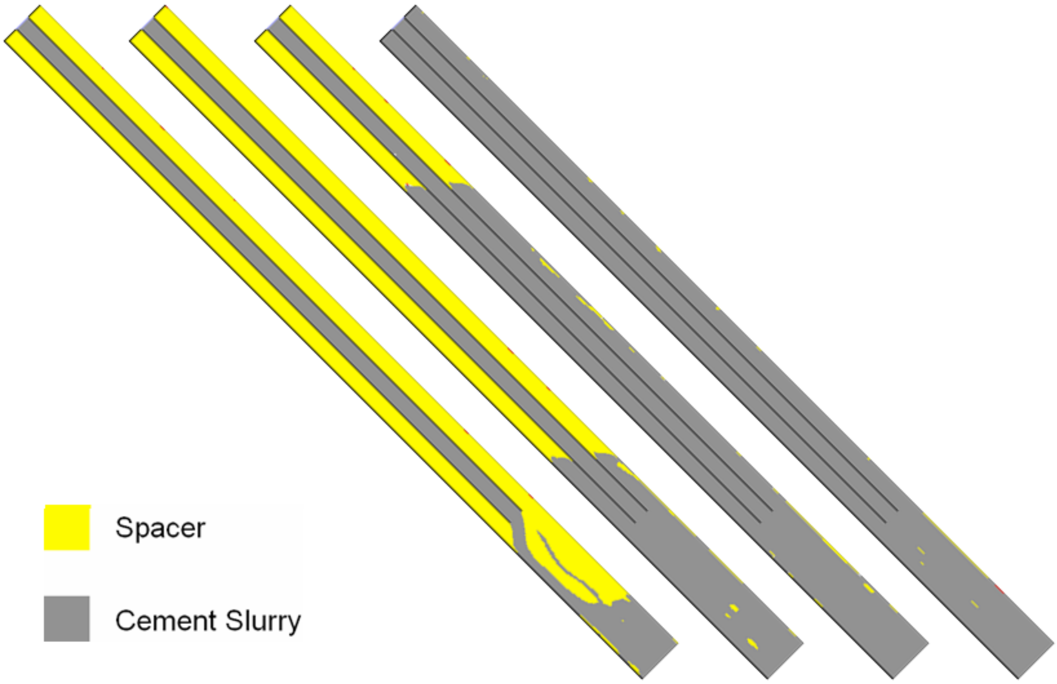

Figure V.24: Interface evolution of the displacement of the spacer material by the cement slurry predicted by the numerical solution of the governing equations.

The numerical simulation images, presented in Fig. V.24, confirm that the displacement of the spacer by the cement slurry was efficient. As in the first replacement four images are shown in this figure: (i) when the spacer exits from the internal tube, (ii) in the beginning of the displacement in the annulus, (iii) in an advanced displacement in the annulus, and (iv) at the end of the pumping operation. Comparing this images with the ones obtained in the first replacement it can be observed that the interface shapes in both replacements are flat, corresponding to an efficient displacement. However, in the first replacement a little more contamination of the displacing material is observed, which confirms the experimental results that show a more efficient displacement in the second replacement (note that in the end of the first replacement the measured density was not equal to the displacing material density).

As in the first replacement, in the second one the higher density and the higher yield stress of the cement slurry compared to the equivalent properties of the spacer were responsible to the efficiency of the displacement obtained.

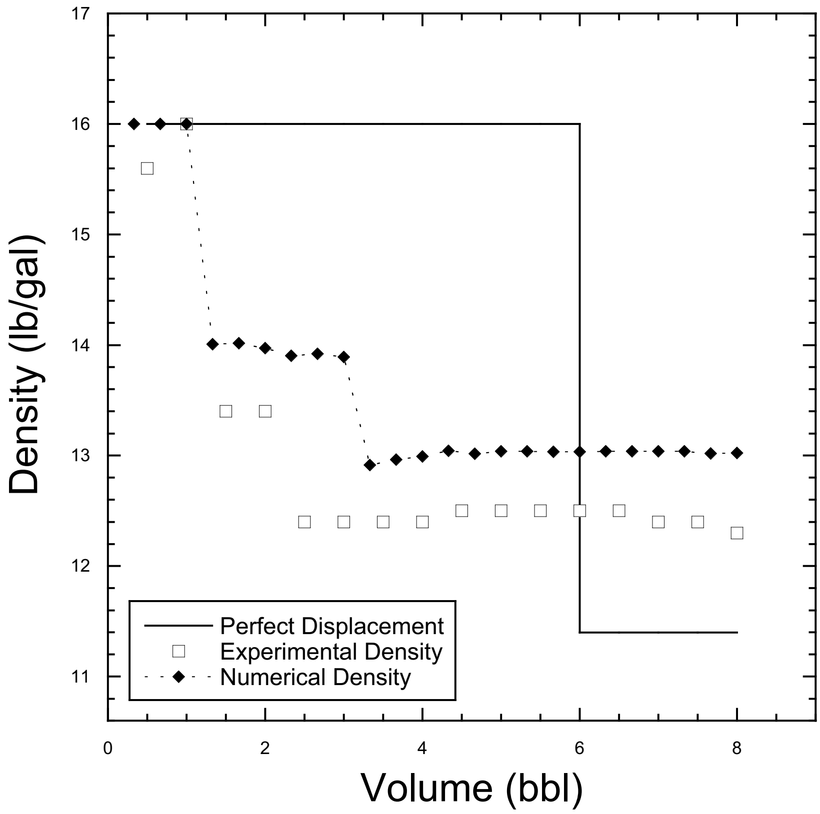

Figure V.25: Experimental and numerical densities versus volume of spacer used to displace the cement slurry, compared with the density that would be obtained if the displacement were perfect.

In the third experiment, 8 bbl of spacer were pumped to displace the cement slurry. As before, Fig. V.25 shows the experimental and numerical density values for this replacement, and a comparison with the density that would be obtained if the displacement were perfect. In this figure, a reduction in the experimental density was observed when only 1.5 bbl were pumped. Also, when 8 bbl of spacer were pumped the experimental density was higher than the spacer one, which indicates fast and severe channeling of the spacer through the cement slurry. From this figure, it can be noted that the majority of the cement slurry remained in the structure. Analyzing the numerical results it can be pointed out that the numerical solution predicted the same trend observed in the experiment, although the numerical values are higher than the ones observed experimentally. More specifically, the numerical solution predicted severe channeling which was observed experimentally.

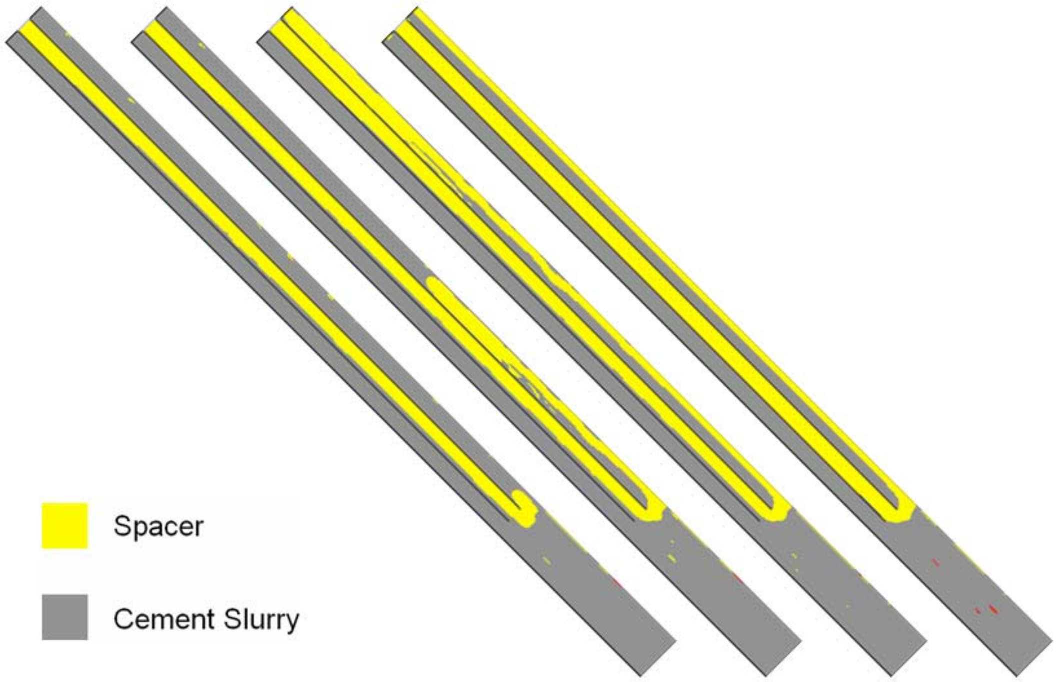

Figure V.26: Interface evolution of the displacement of the cement slurry by the spacer material predicted by the numerical solution of the governing equations.

The images obtained with the numerical simulation, shown in Fig. V.26, confirms what was experimentally observed. The interface shape was not flat which means that the displacement was not efficient. The low displacement efficiency in the third replacement can be attributed to the lower density and yield stress of the spacer (11.4 lb/gal, and 30 lbf/100 ft^2) compared to the cement slurry (16.0 lb/gal, 52 lbf/100 ft^2). The spacer moved only in the upper part of the annulus due to its lower density, and a large volume of the cement slurry was left in the lower part of the annulus.

After the end of the third replacement, the structure was sawed in sections of about 30 cm length and the slices were photographed. The pictures (Fig. V.27) show the cement remaining in the lower part of the structure as predicted in the numerical simulation.

Figure V.27: Pictures of slices of the tube after the cement slurry was displaced by the spacer.

So, in all of the three replacement experiments the displacement of one material by another was well predicted by the numerical simulations which were compared to the experimental results. Also, it was observed that the evaluation of the displacement efficiency by the measured density in the exit of the annulus seems to be a good method.

In the second physical simulation (ii) a cement plug 1 operation was realized in the large scale apparatus. The efficiency of the cement plug operation was evaluated by numerical simulation and also visually by pictures taken after the cement cure.

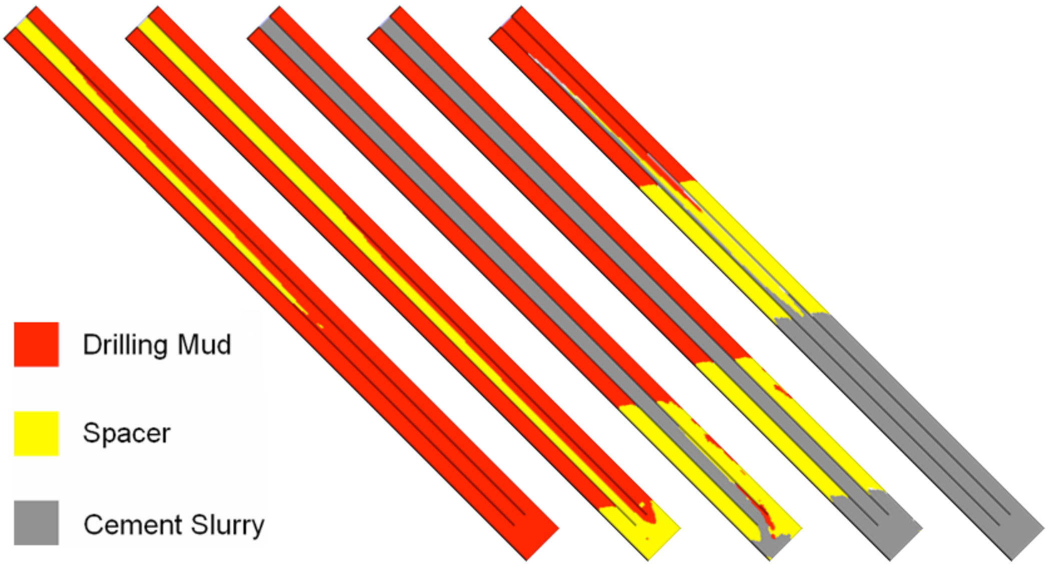

Figure V.28: Interface evolution of the cement plug 1 experiment predicted by the numerical solution of the governing equations.

Fig. V.28 shows the results of the numerical simulation in five steps of the displacement. From this figure it can be noted that the spacer material displaced the drilling mud with a good displacement efficiency and a flat interface. It is also observed that the cement slurry displaced the spacer material in an efficient way. At the end of the cement plug 1 numerical simulation (Fig. V.28), the interior of the tube-annular space was divided in three regions with nearly one material per region (almost without mixture). So the numerical simulation predicted that the cement plug 1 physical simulation would be successful, since there was no significant mixture among materials, and the final internal configuration was equal to the designed one.

(a) (b)

Figure V.29: Pictures of the cement plug 1. (a) The hole plug, and (b) slice located at the top of the plug.

In this experiment (ii), realized in the large scale apparatus, just after pumping all the materials the internal tube was removed. After the cement has been cured, the casing was sawed in sections of about 30 cm and the cement plug photographed. The total length of the cement solidified was 5.4 m as shown in Fig. V.29(a). In this figure two pictures showing the entire cement plug and a its upper part, located between 5.1 m and 5.4 m from the base can be found. Based on the results of the numerical simulation and also on the quality and the length of the cement obtained, it is possible to conclude that the displacements occurred in the operation were efficient. The length of the cement was approximately the same as the one designed, and there was no sign of contamination in the cement which correspond to a successful operation.

At last it can be pointed out that the hierarchy of the density and of the yield stress was essential for the success of the operation, and that the quality of the cement plug obtained was equivalent to the one predicted by the numerical simulation.

The third physical simulation was a cement plug 2 operation (iii) as described in Sec. V.3(c). Fig. V.30 shows the results of the numerical simulation in five steps of the displacement: (i) when the spacer is moving inside the internal tube, (ii) during its initially upward movement in the annulus, (iii) when the cement slurry is entering into the annulus, (iv) when the cement slurry is displacing the materials inside the annulus, and (v) at the end of the operation.

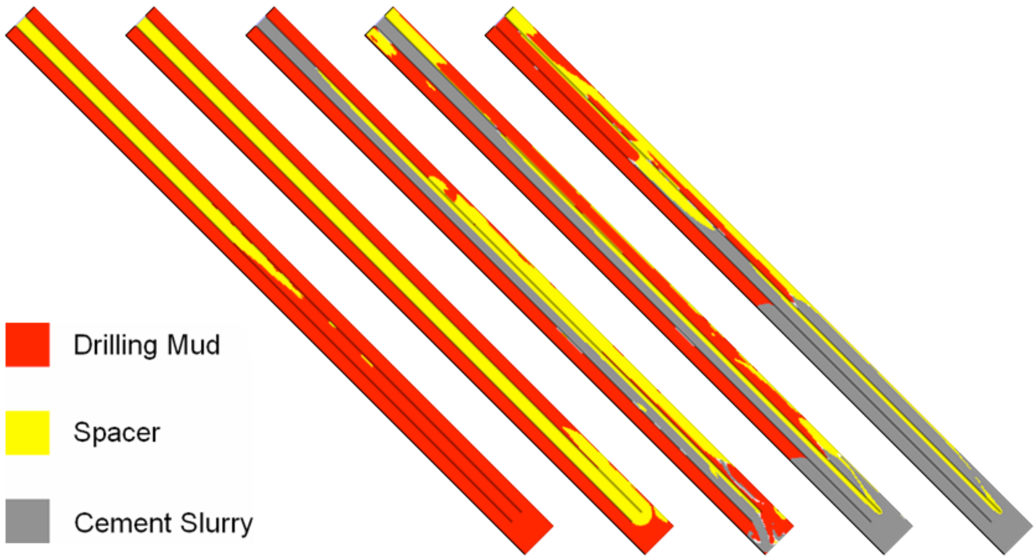

Figure V.30: Interface evolution of the cement plug 2 experiment predicted by the numerical solution of the governing equations.

According to Fig. V.30, the spacer does not enter in the lower part of the annulus, due to its lower density (8.1 lb/gal) when compared to the drilling mud density (10.7 lb/gal). Along the displacement, the spacer creates a channel through the drilling mud at the higher part of the annulus, and at the end of the displacement, the cement plug quality was not satisfactory. There was mixture between the drilling mud and the spacer inside the annulus and the spacer was not able to avoid the contact between the cement slurry and the drilling mud. Therefore, the displacement of the materials was not efficient and the numerical simulation predicted that in the end of the operation the designed cement plug 2 experiment was not successful.

After realizing the cement plug 2 experiment, the casing was sawed in slices of about 30 cm to visually evaluate what happened in the physical simulation. Fig. V.31(a) shows that the extension of solidified cement was much smaller (3.7 m) than the one designed (5 m). Also, it can be seen in Figs. V.31(b) and (c), and V.32 show signs of contamination in the cement as predicted by the numerical simulation.

(a) (b) (c)

Figure V.31: Pictures of the cement plug 2. (a) The hole plug, and (b) and (c) views of the slice located between 2.75 m and 3.05 m from the bottom.

Figure V.32: Pictures of the cement plug 2: views of the slice located between 3.05 m and 3.35 m from the bottom.

The same signs of contamination can be seen in Fig. V.33 of the internal part of the slice located at 2.15 m from the bottom. The signs of contamination showed up from about 95 cm from the bottom. So, for the cement plug 2, both the numerical simulation and the visual inspection of the quality of the plug indicate problems in the displacements resulting in a poor quality plug, mainly caused by the smaller density of the spacer when compared to the drilling mud.

Figure V.33: Pictures of the cement plug 2: views of the slice located between 2.15 m and 2.45 m from the bottom.

V.6 Final Remarks

In this chapter the displacement of viscoplastic materials inside oil wells was analyzed both by experimental investigations and numerical simulations. Four apparatus were built with different scales and the displacement efficiency was experimentally evaluated by the interface shape between materials, captured in pictures, or by the measured density of the mixture of materials at the exit of the annulus.

It was observed, by the results showed in this chapter, that the upward displacement of a material by another in annular space regions becomes more efficient when the density and the viscosity ratio increases, and when the flow rate decreases. It means that the density and the viscosity of the displacing material needs to be higher than the displaced ones to perform a successful operation. This is true since the flow rate is higher enough to minimize the gravity effect in the downward displacement inside the inner tube, so as to avoid channeling due to the density ratio.

Numerical simulations of the experiments realized in two apparatus were performed for comparison with the experimental results. The numerical results could not always predict the interface shape and the density values obtained in the experiments. However, in the same experimental time the numerical simulations could predict if the displacement or the replacement of a material by another were efficient or not, indicating the success or the failure of a certain designed operation. This results illustrate the prediction capability of numerical simulations of displacement operations. Simulating some operations before testing them in practice may save a lot of time and reduce costs dramatically. Therefore, computational non-Newtonian continuum mechanics can be a quite effective tool in the design of displacement operations inside oil wells.

V.7 Note

In this chapter it was realized an analysis of the displacements of viscoplastic materials inside oil wells. Sec. V.1 is a bibliography review about the subject based on previous works of GReo. In Sec. **??** the governing equations of the problem are shown. In Sec. V.3 the experiments realized are described. The pilot scale apparatus 1 was designed by myself based on Dutra [99]. The pilot scale apparatus 2 and the large scale apparatus were built and operated by supervision of Cristiane Miranda from CENPES — PETROBRAS. The experimental results obtained by Cristiane Miranda are shown in this chapter so as to validate the numerical simulation methodology used by myself to perform the numerical solution of displacement problems inside oil wells. Both numerical solution obtained by myself and the experimental results obtained by Cristiane Miranda were presented and published at Offshore Mediterranean Conference and Exhibition 2007 in Ravenna — Italy, and I am co-author of this work. The small scale apparatus presented in this chapter was designed by myself based on my experience with visualization techniques obtained from the pilot scale apparatus 1 and from the experiments described in chapters III and IV. It is important to point out that Renata Pereira helped me in the operation of the pilot scale apparatus 1, and Jane Celnik helped me in the operation of the small scale apparatus. In Sec. V.4 the numerical simulation methodology is described. The results of this research are shown and discussed in Sec. V.5, and some final remarks can be found in Sec. V.6. Prof. de Souza Mendes guided us in this research.